Transport, magnetic, and structural properties of $La_{1-x}M_xMnO_3$ (M=Ba, Sr, Ca) for $0 \leqslant x \leqslant 0.20$

P. Mandal and B. Ghosh
Saha Institute of Nuclear Physics, 1/AF Bidhannagar, Calcutta 700 064, India
(Received 1 November 2002; revised manuscript received 27 March 2003; published 21 July 2003)

At high temperatures both the resistivity (ρ) and thermopower of $La_{1-x}M_xMnO_3$ (M=Ba, Sr, Ca) single crystals can be described well by a small-polaron hopping model. The polaron binding energy decreases while the orbital ordering transition (T_{JT}) to a state with a static Jahn-Teller distortion increases as the ionic size of M reduces from Ba to Ca. With doping (x), T_{JT} decreases and Curie temperature T_C increases. Orthorhombic to rhombohedral transition (T_{OR}) decreases almost linearly with x up to 0.125 and 0.20 for Ba- and Sr-doped samples, respectively. For Ca-doped system, T_{OR} decreases at a much slower rate with x. Unlike Sr-doped sample, both Ca- and Ba-doped systems do not show large drop in ρ at T_C followed by an abrupt increase below T_C for $x=1/8$ doping. Both distortion and disorder due to the difference in size between La and M affect transport, magnetic, and structural properties of manganites. A phase diagram has been constructed from this study.

DOI: 10.1103/PhysRevB.68.014422 PACS number(s): 72.80.Ga, 75.30.−m

I. INTRODUCTION

In perovskite manganites, the orbital, charge, and spin degrees of freedom are considered to be key factors because the huge decrease of resistivity (ρ) is observed in the vicinity of the transition from an insulating charge or orbital ordered phase to a ferromagnetic (FM) metallic state. Parent compounds $RMnO_3$ (R= rare-earth ions) are insulators and show C-type orbital ordering due to static Jahn-Teller (JT) interaction below a transition temperature T_{JT} where $d_{3x^2-r^2}$ and $d_{3y^2-r^2}$ e_g orbitals are alternately aligned in the ab plane and the planes are stacked along the c axis. This particular orbital arrangement is responsible for strong in-plane FM coupling and weak antiferromagnetic (AFM) coupling between the planes, and prevents electron hopping between Mn^{3+} sites. As the concentration of Mn^{4+} in $R_{1-x}M_xMnO_3$ increases by replacing R with divalent ions M, the electron transfer with spin memory between Mn^{3+} and Mn^{4+} sites becomes prevalent. This coherent hopping of carriers competes with the cooperative interaction responsible for orbital or charge ordering and as a consequence, a rich phase diagram has been observed.

Prototype $La_{1-x}Sr_xMnO_3$ (LSMO) is well studied over a narrow range of doping around $x=0.125$, where a sequence of transitions occur as a function of temperature. In the lightly doped region, transport, magnetic, and structural properties revealed many interesting features and a rich phase diagram.[1–16] In contrast, there are no detail analyses of transport and magnetic properties as function of doping and temperature, particularly in the vicinity of structural and magnetic phase transitions on single crystals of lightly doped $La_{1-x}Ba_xMnO_3$ (LBMO) and $La_{1-x}Ca_xMnO_3$ (LCMO). Dabrowski *et al.*[17] have made a careful study of the structural, magnetic, and electronic properties of LBMO polycrystalline samples for $0.10 \leqslant x \leqslant 0.24$. However, this study could not reveal all the finer details of the several transitions and crossovers that occur at low temperatures with the variation of composition. For example, they observed that the orthorhombic to rhombohedral structural transition T_{OR} decreases faster with x in LBMO as compared to LSMO. However, for $x>0.125$ we observe that T_{OR} decreases at a faster rate in LSMO than in LBMO. One needs structural data at low temperature to observe this difference between the two systems. Also, there are some discrepancies in reported results on polycrystalline samples, possibly due to the variation of oxygen content and the presence of grain boundaries.[17,18] In the case of single crystals, oxygen content is very close to 3 and the effect due to grain boundaries is absent. Good quality single crystals are also required to observe the anomaly in the transport and magnetic properties in the vicinity of structural transition temperature. If the anomaly is very weak then it may not be seen in polycrystalline samples. For Ca-doped system most of the reported studies are concentrated for doping $x \geqslant 0.125$.[19] It is also important to investigate how the transport and other properties evolve in $La_{1-x}Ca_xMnO_3$ when the doping is changed by small steps (Δx) around $x=0$ and beyond.

In this work, we present the transport, magnetic, and structural properties of $La_{1-x}M_xMnO_3$ (M=Ba, Sr, Ca) single crystals for $0 \leqslant x \leqslant 0.20$. Resistivity has been measured both above and below the structural phase-transition temperature. The temperature dependence of magnetization and x-ray diffraction have been studied only for some selected samples. For LSMO we have also used data from our earlier report.[20]

II. SAMPLE PREPARATION AND EXPERIMENTAL TECHNIQUE

Single crystals were grown by floating-zone method.[20] Both x-ray and neutron powder diffraction were used to determine the structure and verify the crystal quality. All the samples are single phase. The lattice parameters for LBMO system were determined, by powder x-ray diffraction, down to 80 K. The high-temperature resistivity was measured in vacuum in order to prevent oxidation. Magnetic properties were measured in the temperature range 2–300 K using a superconducting quantum interference device magnetometer (Quantum Designs).

III. EXPERIMENTAL RESULTS AND DISCUSSION

A. Transport properties

In manganites, the formation of small lattice polarons due to strong electron-phonon coupling and their properties in the vicinity of ferromagnetic transition and beyond have been reported from different measurements.[8,9,20–25] In the case of small-polaronic conduction, the transport mechanism at high temperatures is the thermally activated hopping of carriers, with the conductivity (σ) and mobility (μ) given by[24–27]

$$\sigma(T)=\sigma_0 e^{(-E\rho/k_BT)} = \frac{c(1-c)e^2}{\hbar a} \times\left(\frac{T_0}{T}\right)^n \exp\left(-\frac{E_0+W_H-J^{3-2n}}{k_BT}\right), \quad (1)$$

$$\mu(T)=\frac{c(1-c)ea^2}{\hbar}\left(\frac{T_0}{T}\right)^n \exp\left(-\frac{W_H-J^{3-2n}}{k_BT}\right), \quad (2)$$

where a is the hopping distance of polaron, J the transfer integral, c the polaron concentration, E_0 the energy difference between two sites of identical lattice distortions with and without the charge carrier, and W_H is one half of polaron formation energy E_p. When the polaron hops rapidly between two sites with identical configuration, it is termed as adiabatic hopping. In this regime, n is equal to 1 and $k_BT_0=h\nu$, where ν is the longitudinal optical-phonon frequency of the system. In the case of nonadiabatic limit, $n=3/2$ and $k_BT_0=(\pi J^4/4W_H)^{1/3}$.

To elucidate the nature of charge transport, we have plotted $\log_{10}(\rho/T)$ versus $1/T$ in Fig. 1(a) for Ba-, Sr-, and Ca-doped samples with $x=0.05$. ρ shows a semiconductinglike behavior for all the three samples. With increasing temperature, a sharp decrease in ρ is observed at T_{JT} where the system undergoes a structural phase transition from O'- to O-orthorhombic. The values of T_{JT} are 552, 607, and 618 K for Ba-, Sr-, and Ca-doped samples, respectively. Sequence $T_{JT}(\mathrm{Ba})<T_{JT}(\mathrm{Sr})<T_{JT}(\mathrm{Ca})$ suggests that the dopant with larger ionic size affects the orbital ordering temperature strongly. For a given x, the Ba-doped sample has larger tolerance factor (t) as compared to Sr- and Ca-doped compounds due to the larger ionic radius of Ba. At high temperature, well above T_{JT}, there is another anomaly at T_{OR} due to O-orthorhombic to rhombohedral phase transition but this anomaly is much weaker than that at T_{JT}. Similar to T_{JT}, T_{OR} also increases from LBMO to LSMO to LCMO.

All curves in Fig. 1(a) are linear over a wide range of temperature below T_{JT}. But the slope of the curves, i.e., the activation energy (E_ρ) decreases from Ba to Sr to Ca doping. Similar behavior has also been observed for samples with other doping levels. E_ρ for Sr-doped sample is $\sim$260 meV, which is about 7%–9% lower and 11%–13% higher than E_ρ for Ba- and Ca-doped samples, respectively. Similar to the Sr-doped samples,[20] E_ρ for Ca- and Ba-doped samples is almost doping independent up to 0.10 and then decreases fast with further increase of x. The resistivity data can also be fitted well with nonadiabatic hopping of polarons. However, due to the presence of the exponential temperature-dependent factor with large E_ρ, the fit is insensitive to the small difference in the T dependence of prefactor σ_0 in Eq. (1). Nevertheless, the small value of σ_0 for $x\leqslant 0.05$ samples suggests that the hopping is nonadiabatic in this low doping range and adiabatic for $x>0.05$. The nonadiabatic value of E_ρ is 6% to 8% higher than the adiabatic one.

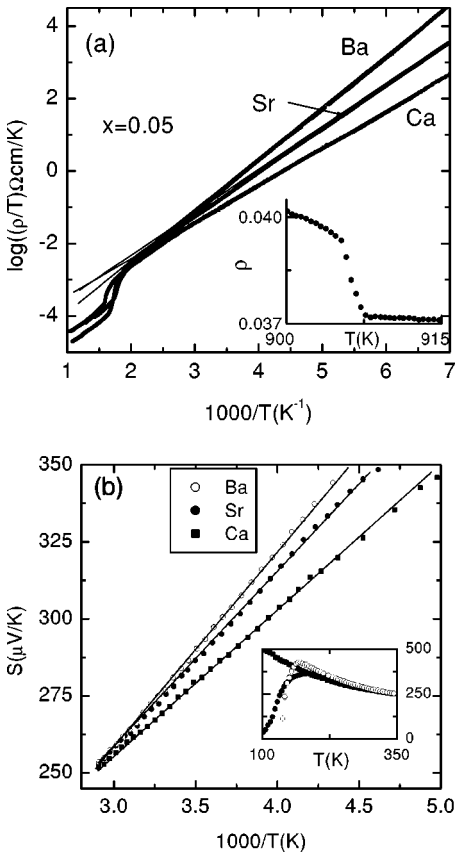

FIG. 1. (a) Temperature dependence of resistivity data in the adiabatic limit. Inset: Resistivity anomaly in the vicinity of orthorhombic to rhombohedral structural phase transition for 5% Ca-doped sample. (b) S vs $1000/T$ plot for the above three samples. Inset: T dependence of S down to 100 K. S for Ba-doped sample has been shifted upward by 100 μV/K. The solid lines in Figs. 1(a,b) are fits in the high-temperature regime for polaronic conduction [Eqs. (1) and (3) in the text].

In order to know how W_H depends on the type of dopant, it is important to determine E_0 in Eq. (1). Measurements of thermopower (S) will provide E_0. As the carrier hops from one locally distorted site to another that has been thermally activated, thermopower of small-polaronic system is determined by barrier energy E_0 similar to band semiconductor[24]

$$S=(k_B/e)\frac{E_0}{k_BT}+S_0, \quad (3)$$

where S_0 is a constant. In Fig. 1(b), S has been plotted as a function of $1000/T$ for $x=0.05$ doping. Above 200 K, S is

approximately linear for all the three samples. The values of E_0 determined from the high-temperature linear part are 70, 61, and 49 meV for LBMO, LSMO, and LCMO, respectively. Thus, similar to E_ρ, E_0 also decreases from LBMO to LSMO to LCMO. Using these values of E_0 and neglecting J, we can calculate that polaron binding energy $E_P = 420$, 399, and 370 meV for LBMO, LSMO, and LCMO samples, respectively, for 0.05 doping. So, the polaron binding energy is slightly higher for LBMO system. At this moment we do not know why E_P is higher for LBMO. One possible reason for this small discrepancy is the contribution from the hopping due to disorder. In the presence of small disorder the activation energy E_ρ contains an additional term $1/2W_D$ other than E_0 and J.[27] Due to the large difference in ionic radii between Ba and La the effect due to disorder is expected to be slightly larger in the case of LBMO.

Though $\rho(T)$ for all the samples ($0 \leqslant x \leqslant 0.20$) have been studied, here we present the results of some selected samples close to $x = 0.125$ (Fig. 2). We have chosen these concentrations because the electrical resistivity is strongly influenced by several successive structural and magnetic phase transitions close to this doping. It has already been mentioned that there are several reports on transport properties of Sr-doped samples close to $x = 0.125$. However, we have included the resistivity and thermopower data for 0.125 and 0.15 Sr-doped samples in the present study to compare and contrast these results with those of Ca- and Ba-doped systems with the corresponding value of doping. It is clear from Fig. 2(a) that for $x = 0.125$, the effect of structural and magnetic transitions on $\rho(T)$ for LCMO and LBMO are slightly different from that observed in LSMO. The T dependence of ρ for 0.125 LSMO is consistent with the earlier reports.[1,5] ρ decreases by about 60% between T_C and T_{CO} and then increases sharply just below T_{CO}. On the other hand, only 1% to 2% resistivity drop has been observed below T_C for both LCMO and LBMO. Although LCMO undergoes a structural transition to pseudocubic phase below T_{CO}, similar to LSMO, no abrupt increase of ρ has been observed in LCMO.[28] In LSMO, a long-range polaron ordering has been reported below T_{CO}[9] and this transition is of first order in nature.[3,10,16] However, LCMO does not show any long-range ordering of polarons but short-range correlation has been detected for $0.15 \leqslant x \leqslant 0.20$ (Ref. 9). For LBMO there is no such study on polaron formation and polaron-polaron correlation close to 1/8 doping. Nevertheless, the nature of resistivity increase below T_{CO} in LBMO is quite similar to that of LCMO system. This phenomenon indicates that ionic size plays an important role in the nature of resistivity increase below T_{CO}, i.e., at an optimum ionic size, ρ shows a sharp jump. Also, the anomaly at T_{JT} is much weaker for LBMO and LCMO than that observed in LSMO.

ρ for LBMO, LSMO, and LCMO samples with $x = 0.15$ first decreases below T_C but, on further cooling, shows a smooth upturn with a low-temperature insulating behavior [Fig. 2(b)]. ρ does not increase abruptly at low temperatures below T_{CO} in these samples. A weak feature or a change in slope has been observed at $T_{OR} = 370$ and 265 K for LSMO and LBMO samples, respectively. No anomaly due to the static JT distortion has been observed in these samples. On the other hand, T_{JT} is as high as 300 K for LCMO. T_{OR} for both 0.125 and 0.15 LCMO samples are 806 and 777 K, respectively.

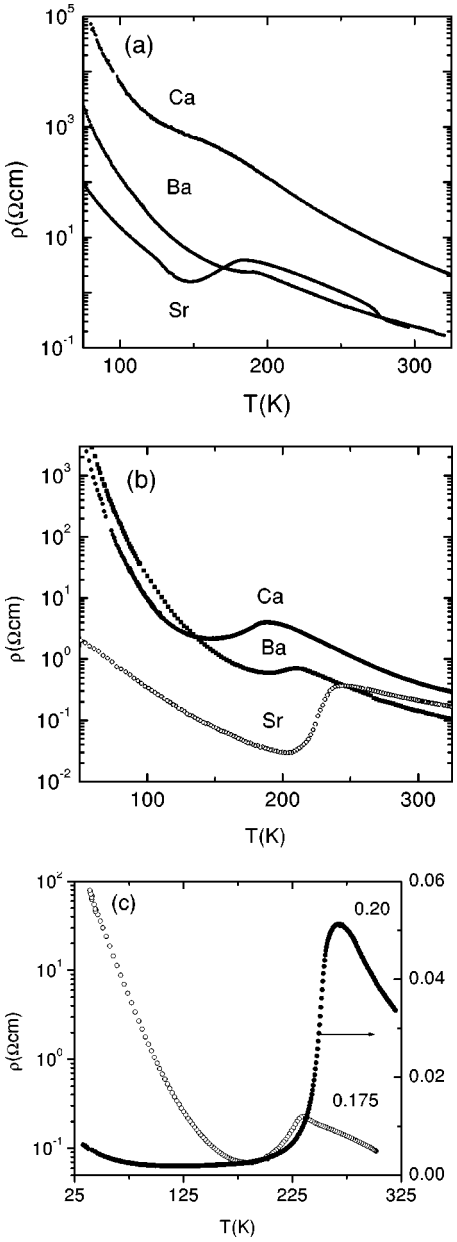

FIG. 2. Temperature dependence of ρ for $La_{1-x}A_xMnO_3$ samples with different x: (a) $x = 0.125$, (b) $x = 0.15$, and (c) for Ba-doped samples with $x = 0.175$ and 0.20.

For LBMO system, the behavior of $\rho(T)$ for $x = 0.175$ and 0.20 samples are shown in Fig. 2(c). ρ for $x = 0.175$ sample decreases below T_C and then increases at low temperatures. However, at low temperatures, the nature of increase of ρ is very different from that for $x = 0.15$ sample. The $\ln(\rho)$ versus $1/T$ plot (not shown) shows a saturationlike behavior at low temperatures. Thus, this sample is close to the critical doping (x_{MI}) at which metal to insulator (MI) transition occurs. At $x = 0.20$, the T dependence of ρ changes dramatically. In the FM region ρ decreases with decreasing

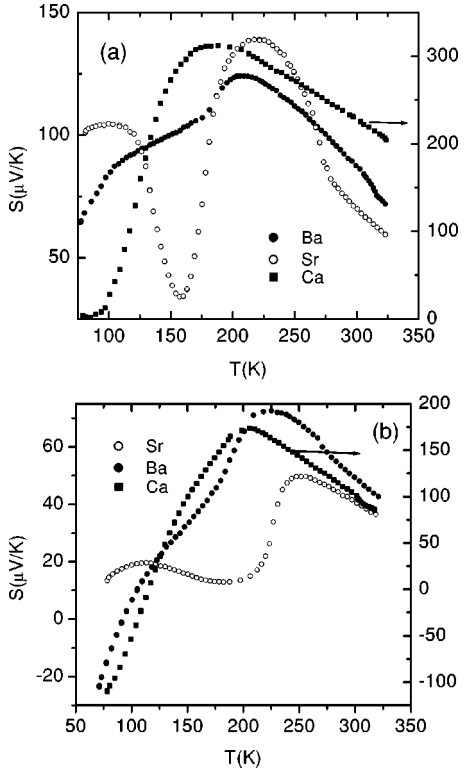

FIG. 3. Temperature dependence of thermopower for $La_{1-x}A_xMnO_3$ with different x: (a) $x=0.125$, and (b) $x=0.15$.

T. The small upturn at low temperatures may be due to the weak localization. Thus, for LBMO system, the MI transition occurs at around $x_{MI}=0.20$. This value for x_{MI} is slightly higher than that reported for polycrystalline samples.[17] A small thermal hysteresis between heating and cooling cycles has been observed at around $T_{OR}=170$ K for $x=0.20$ sample. For LCMO system we have not seen MI transition up to $x=0.20$. Neutron diffraction and other studies show that T_{JT} is very close to T_C at $x=0.15$ and 0.20 for LSMO and LCMO, respectively, and slightly above these values of doping T_{JT} disappears and the systems become metallic.[6,28] Thus, MI transition in both LSMO and LCMO may be driven by the suppression of static JT ordering. However, in the case of LBMO, though T_{JT} decreases at a faster rate as compared to LSMO and T_{JT} is much lower than T_C for $x \geqslant 0.125$, the MI transition occurs at a higher value of x_{MI}. Other localization phenomena, such as dynamic JT distortion in the *O*-orthorhombic phase and the disorder due to the size mismatch between La and Ba ions, may play important role in shifting the x_{MI} to higher value in LBMO. It has been shown in a later section that this disorder increases with Ba-doping and acts like a JT distortion.

Figure 3 shows the T dependence of S for LBMO, LSMO, and LCMO with $x=0.125$ and 0.15. $S(T)$ for 0.125 LSMO is consistent with the previous report.[10] Unlike LSMO, the T dependence of S for 0.125 LCMO sample is quite simple. In the paramagnetic (PM) phase, on cooling, S increases, down to T_C, and then decreases very rapidly in the FM state. The behavior of $S(T)$ for 0.125 LBMO is somewhat in between LCMO and LSMO. S increases slowly with decreasing T in the PM state and then starts to decrease below T_C. Below T_C, closer inspection reveals different temperature regimes depending on the nature of $S(T)$. For this sample, S neither decreases very rapidly below T_C, like LCMO, nor increases abruptly below T_{CO} as in the case of LSMO. S is positive for all the three samples in the measured temperature range. Samples with $x=0.15$ show an overall decrease of S due to the increase of carrier density. For this concentration also, one can see that at low temperatures the nature of T dependence of S for LBMO and LCMO are different from that of LSMO. At low temperature, S is large and negative for LCMO while S is small and negative for LBMO. For LSMO, S remains positive over the whole temperature range and the overall magnitude is smaller than that for other two systems. $S(T)$ shows weak anomalies at T_{JT} for LCMO and at T_{OR} for LBMO. As in the case of resistivity, we have not seen any anomaly in $S(T)$ due to JT transition for LBMO above $x=0.125$. For both $x=0.125$ and 0.15 LCMO, the nature of T dependence of S is quite similar and the large value of S is consistent with the high resistivity.

B. Magnetic properties

Magnetic properties of some selected LBMO samples will be discussed here. Magnetization $M(T)$ for $x=0.125$, 0.15, and 0.20 samples at low field (20 Oe) are shown in Fig. 4(a). With decreasing temperature all the samples show a sharp transition from PM to FM state at T_C. The sharp transition indicates that the samples are of good quality with homogeneous distribution of Ba ion. For $x=0.125$, 0.15, and 0.20, the values of T_C are 200, 218, and 268 K, respectively. For $x=0.20$ sample, on cooling, M shows a small steplike decrease at around T_{OR}. T_C for $x=0.125$ and 0.15 samples are slightly lower but sharper than that observed in polycrystalline samples.[17] This discrepancy may be due to the slightly higher oxygen content than the stoichiometric value 3 in polycrystalline samples. $M(H)$ for these samples increases sharply at low fields and shows almost saturationlike behavior above 0.3–0.5 T [Fig. 4(b)]. The value of the spin only moments (μ_S) calculated at 5 T for 0.125, 0.15, and 0.20 samples are 3.88, 3.77, and 3.60 μ_B, respectively. The theoretical values of μ_S, calculated using the spin only moments of Mn^{3+} ($4\mu_B$) and Mn^{4+} ($3\mu_B$) ions, are 3.88, 3.85, and 3.80 μ_B, respectively, for $x=0.125$, 0.15, and 0.20. This shows an excellent agreement between experimental and theoretical values, particularly for 0.125 and 0.15 samples. Though the FM transition is sharp and the spin only moment is very close to the theoretical value for 0.125 sample, one cannot completely rule out the presence of a weak canted AFM state at low temperatures below T_C, which becomes fully spin polarized when a small magnetic field 0.10–0.30 T is applied. In contrast to LSMO, no abrupt change has been observed in $M(T)$ just below T_{CO} for 0.125 LBMO.[11,16]

We have measured the ac susceptibility for $x=0.125$ sample to see any effect of structural transition on magnetic properties [Figs. 4(c), 4(d)]. Both real (χ') and imaginary (χ'') parts of the ac susceptibility increase sharply at T_C and show a peak just below T_C. However, χ'' exhibits some additional features well below T_C. χ'' shows a sharp peak at

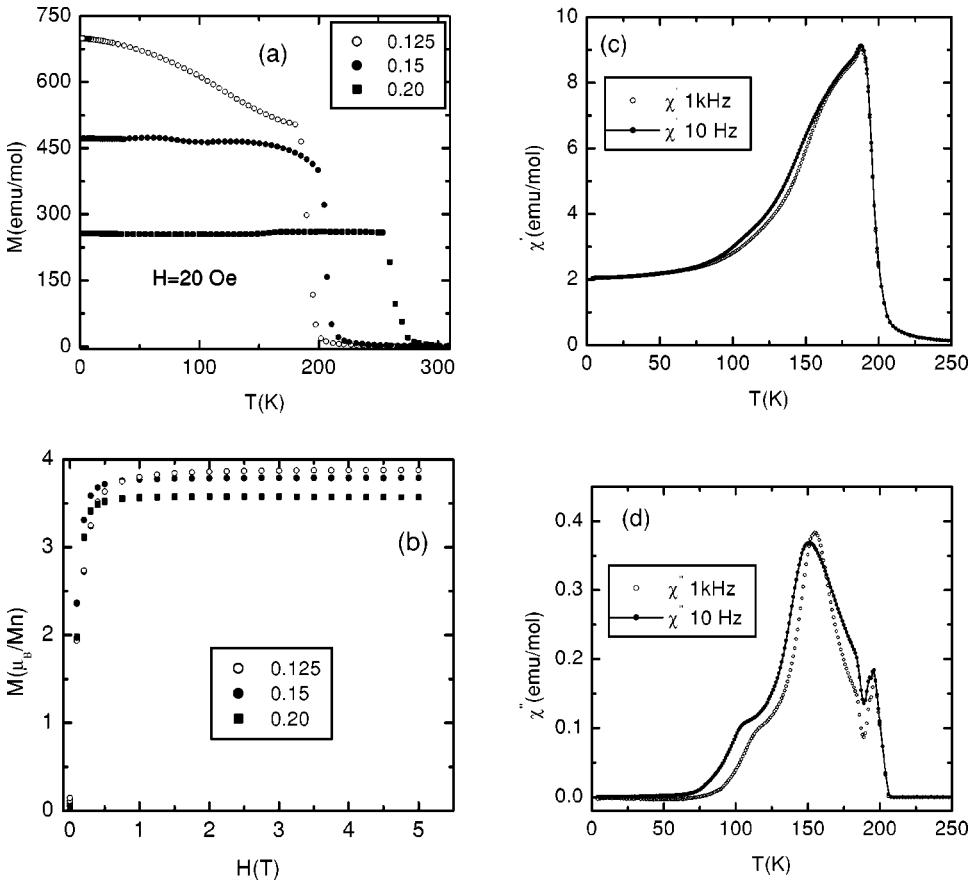

FIG. 4. (a) Temperature dependence of low-field dc magnetization for $La_{1-x}Ba_xMnO_3$ samples with $x=0.125$, 0.15, and 0.20. (b) Magnetization as a function of magnetic field for $x=0.125$, 0.15, and 0.20 samples. (c) Temperature dependence of real part of ac susceptibility (χ') for 0.125 Ba-doped sample. (d) Temperature dependence of imaginary part of ac susceptibility (χ'') for 0.125 Ba-doped sample.

the structural transition $T_{JT}=150$ K and a shoulderlike feature at around 100 K. Though $\chi'(T)$ and the dc M do not show any noticeable feature around 100 K but $d\chi'/dT$ and dM/dT show respectively, a broad maximum and a shallow minimum around 150 K. The peak at 150 K shifts towards higher temperature and becomes sharper with frequency. However, the peak just below T_C does not shift with frequency.

The dependence of T_C on doping has been shown in Fig. 5 for $0.10 \leqslant x \leqslant 0.20$. Figure 5 shows that T_C increases with x for all the three systems but at a given doping, T_C also depends on the type of dopant. It has been shown that in

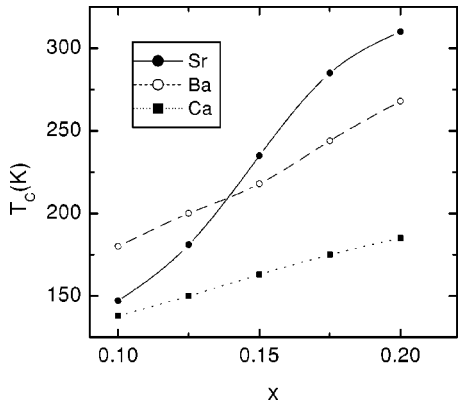

FIG. 5. The dependence of ferromagnetic Curie temperature T_C on doping ($0.10 \leqslant x \leqslant 0.20$) for Ba-, Sr-, and Ca-doped systems.

$AMnO_3$ perovskite T_C is mainly affected by the average size of the A-site cations, $\langle r_A \rangle$ ($=\Sigma y_i r_i$) and by the A-site cation size variance σ^2 ($=\Sigma y_i r_i^2 - \langle r_A \rangle^2$), where y_i is the fractional occupancy of the atom with ionic radius r_i.[29] To quantify the effect of these two phenomena on T_C, Rodriguez-Martinez and Attfield[29] proposed an empirical relation between T_C and $Q_0[=(r_A^0 - \langle r_A \rangle)]$ and σ:

$$T_C(\langle r_A \rangle, \sigma) = T_C(r_A^0, 0) - p_1 Q_0^2 - p_2 \sigma^2, \tag{4}$$

where r_A^0 is the ideal A-site radius for an undistorted cubic perovskite with $t=1$ and is a function of x, $T_C(\langle r_A \rangle, \sigma)$ is the observed FM transition, $T_C(r_A^0, 0)$ is the ideal temperature of FM transition of the cubic perovskite, and p_1 and p_2 are constants. Equation (4) describes approximately the variation of T_C with the increase of ionic size, as the dopant changes from Ca to Sr to Ba for a given x. To calculate $\langle r_A \rangle$ the ionic radii for 12-coordinated La (1.36 Å), Ca (1.34 Å), Sr (1.44 Å), and Ba (1.61 Å) are used.[30] We have estimated $p_1 \sim 7 \times 10^3$ KÅ^{-2}, $p_2 \sim 10^3$ KÅ^{-2}, and $T_C(r_A^0, 0) = 235 \pm 10$ K for $x=0.10$ and the corresponding values for $x=0.20$ are 2×10^4 KÅ^{-2}, 10^4 KÅ^{-2}, and 425 ± 20 K. As the ionic size of Ca is very close to La, the effect of disorder (σ^2) on T_C suppression is negligible over the whole range of doping for LCMO. However, due to the smaller size of Ca as compared to r_A^0, the second term in Eq. (4) is quite large and increases rapidly with x and as a consequence, T_C in this system is much lower than $T_C(r_A^0, 0)$. For LSMO too, T_C suppression

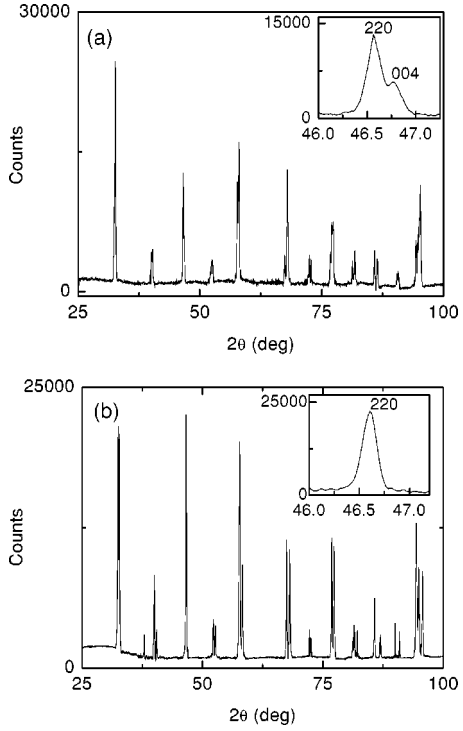

FIG. 6. X-ray diffraction patterns for $x=0.15$ Ba-doped sample at: (a) 200 K and (b) 350 K. The insets in the figures demonstrate the evolution of (220) peak with temperature.

is mainly due to the smaller average size of the *A*-site cations than r_A^0. However, the effect due to both the smaller average size and the size variance of the *A*-site ion on T_C are comparable in LBMO. For $x>0.125$, the last term in Eq. (4) is larger than the second term and increases rapidly with *x* and as a consequence, T_C in LBMO does not increase as fast as in LSMO above this doping. This explains why T_C is higher for LSMO than for LBMO above $x=0.125$ in Fig. 5.

C. Structural analysis

Figure 6 shows the x-ray diffraction patterns at 200 and 350 K for 0.15 LBMO. All the peaks can be indexed with orthorhombic unit cell at 200 K and with rhombohedral unit cell at 350 K. With increasing temperature, *O*-orthorhombic (space group $Pbnm$) to rhombohedral (space group $R\bar{c}3$) phase transition occurs at around 265 and 315 K for $x=0.15$ and 0.125, respectively. The insets in the figures demonstrate the evolution of peaks at around $2\theta=47°$ as the system undergoes phase transition from orthorhombic to rhombohedral. In the rhombohedral phase there is only one intense and symmetrical peak (220) whereas in the orthorhombic phase it splits into two (004,220) relatively weaker peaks. Similar behavior has also been observed for 0.125 sample.

The *T* dependence of the lattice parameters calculated from the diffraction patterns are shown in Fig. 7. To compare with *a* and *b* we have actually plotted $c/\sqrt{2}$. Lattice parameters *a* and $c/\sqrt{2}$ of the orthorhombic phase can be extrapolate to the equivalent lattice parameters *a* and c_{eq} of the

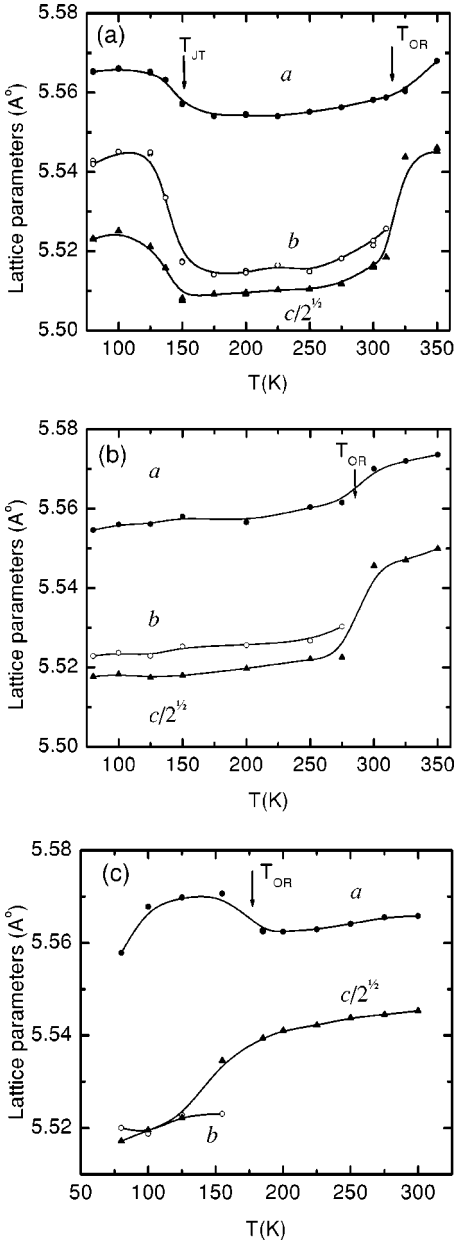

FIG. 7. The temperature variation of lattice parameters *a*, *b*, and *c* for Ba-doped samples: (a) $x=0.125$, (b) $x=0.15$, and (c) $x=0.20$. Structural phase transition temperatures T_{JT} and T_{OR} are marked by the arrows.

rhombohedral phase at higher temperature. The equivalent $c/\sqrt{2}$ for the rhombohedral phase, $c_{eq}=c_O/\sqrt{2}$, is obtained from: $a_H=a_O$, $b_H=1/2(a_O-b_O-c_O)$, and $c_H=2a_O+c_O$, so that $18c_{eq}^2=c_H^2+12a_H^2$ (subscripts *H* and *O* stand for hexagonal and orthorhombic, respectively).[31,32] For $x=0.125$, the lattice parameters in the *O*-orthorhombic phase decrease slowly with *T*, down to 150 K and then display a small but abrupt increase at 150 K due to *O*- to *O′*-orthorhombic transition. Unlike LSMO and LCMO, we have not seen any *O′*-orthorhombic to pseudocubic phase transition below T_{CO} for 0.125 LBMO sample.[5,28] This suggests that the transition to pseudocubic phase either takes place below 80 K or both *O*- to *O′*-orthorhombic and *O′*-orthorhombic to pseudocubic

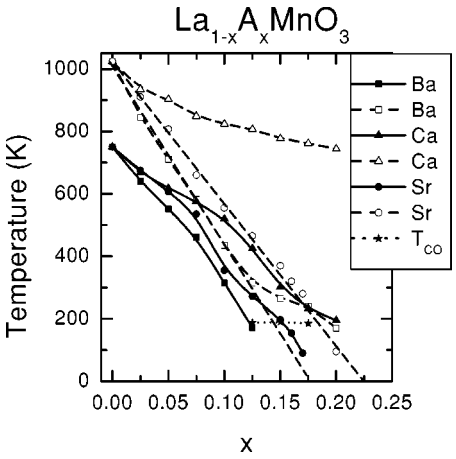

FIG. 8. Temperatures, T_{OR} (open symbol), T_{JT} (filled symbol) and T_{CO} (star), determined from transport, magnetic, and structural properties (see text) are plotted as a function of doping x. The lines through the symbols are the guide to the eyes.

transitions occur so close to each other that we are unable to separate these two transitions. The T dependence of lattice parameters of LBMO in the O' phase are also different from that of Ca- and Sr-doped samples with $x=0.125$. In the latter systems a increases and c decreases sharply while for the 0.125 LBMO sample both a and c increase below T_{JT}.[5,6,28]

The T dependence of lattice parameters for $x=0.15$ in the O-orthorhombic phase is similar to that of 0.125 sample. The lattice parameters of this sample show a small but sharp increase just above T_{OR}. However, for $x=0.20$ sample, c increases whereas a decreases at T_{OR}. We have not seen any O- to O'-orthorhombic transition down to 80 K for $x \geqslant 0.15$. Both T dependence of lattice parameters and the small difference between b and $c/\sqrt{2}$ for Ba-doped 0.125 sample are comparable to that of Sr-doped 0.165 sample. Also, T_{OR} for these two samples are almost same ($\sim$315 K). It has been suggested that the structural phase transition is governed by the tolerance factor.[17] The same T_{OR} for 0.125 LBMO and 0.165 LSMO is due to the same value of $t=0.97$ for both the samples. Though t increases faster with x for LBMO as compared to LSMO, T_{OR} decreases at a much slower rate with x above 0.125 in the former system than the latter. As in the case of magnetic property, the disorder due to the larger ionic size of Ba may be responsible for the slower decrease of T_{OR} in LBMO. Due to the A-site cation disorder there is a random displacement of oxide ions from their mean crystallographic position with mean random displacement $Q_r=\sigma(=\sqrt{\sigma^2})$. This Q_r is related through the lattice strain term in the JT part of the Hamiltonian, $K(Q_r^2+Q_0^2)$; here $Q_0=(r_A^0-\langle r_A\rangle)$ is the change in Mn-O bond length due to the static JT effect.[29] For Ba-doped samples above $x=0.125$, $Q_r>Q_0$ (at $x=0.20$, $Q_r>2Q_0$). Thus the local deformations of the MnO_6 octahedra due to the A-site disorder acts as ''preformed JT distortions,'' (as described in Ref. 29) that favor both carrier localization and orthorhombic structure.

D. Phase diagram

Based on transport, magnetic, and structural properties discussed above, a structural phase diagram for Ba-, Sr-, and Ca-doped systems has been constructed (Fig. 8). The magnetic phase diagram T_C versus x for $0.10 \leqslant x \leqslant 0.20$ has already been presented in Fig. 5. For LBMO, T_{OR} decreases almost linearly with x up to $\sim$0.125. Above $x=0.125$ T_{OR} decreases at a slower rate than linear. However, for LSMO T_{OR} decreases approximately linearly up to as high as $x=0.20$. In the linear region, T_{OR} decreases at a faster rate in LBMO than in LSMO and T_{OR} extrapolated to 0 occurs at $x=0.175$ and 0.225 for the former and the latter systems, respectively. Due to the slower decrease of T_{OR} for LBMO above $x=0.125$, the orthorhombic to rhombohedral transition is higher for LBMO than LSMO above $x=0.175$. For LCMO, T_{OR} decreases slowly with x and develops a saturationlike behavior at higher Ca concentration. In the doping range 0–0.20, T_{OR} did not decrease below 745 K. This behavior is consistent with the orthorhombic structure of $CaMnO_3$ well above the room temperature.[33] Over the whole doping range, T_{JT} decreases faster for LBMO as compared to LSMO and LCMO. We have not seen any indication of static JT effect for LBMO for $x \geqslant 0.15$. Detailed structural analysis, down to low temperatures, is important to see whether JT effect vanishes at $x=0.15$ or not. For LBMO, the dependence of T_{CO} on carrier density is also shown in the figure. We define the temperature where $\rho(T)$ shows a minimum slightly below T_C, as T_{CO}. Below T_{CO}, the ferromagnetic phase is insulating. For LBMO T_{CO} is almost flat over the doping $0.125 \leqslant x \leqslant 0.175$.

IV. CONCLUSIONS

Analysis of resistivity and thermopower suggests that the transport is governed by the thermally activated hopping of small polarons. Irrespective of the size of A-site ion, E_ρ is almost independent of x up to 0.10 and then decreases above this value of x. Both E_ρ and E_P decrease slightly as divalent ion M changes from Ba to Sr to Ca. In contrast to Sr-doped sample, on cooling, both Ca- and Ba-doped samples do not show large drop in ρ below T_C followed by an abrupt increase at T_{CO} for $x=1/8$ doping. T_{JT} decreases more rapidly with x for LBMO as compared to LSMO and LCMO. T_{OR} shows linear behavior up to $x=0.125$ and 0.20 for LBMO and LSMO systems, respectively. The decrease of T_{OR} in LBMO is slower than linear for $x>0.125$. For LCMO system T_{OR} does not decrease monotonically with x. The differences in transport, magnetic, and structural properties between Ba- and Sr-doped samples above $x=0.125$ are strongly coupled with the distortion (t) and disorder (σ) due to the A-site lattice mismatch. The higher value of x_{MI} in LBMO as compared to LSMO may also be due to this disorder. A phase diagram has been constructed to show the variation of T_{OR}, T_{JT}, T_C, and T_{CO} with doping x.

ACKNOWLEDGMENTS

We thank A. Pal, D. Vieweg, and M. Müller for technical supports and Prof. A. Loidl for using the x-ray and magnetic measurements facilities in his laboratory. One of us (B.G.) acknowledges the financial support from INSA.

[1] A. Urushibara, Y. Moritomo, T. Arima, A. Asamitsu, G. Kido, and Y. Tokura, Phys. Rev. B **51**, 14 103 (1995).
[2] Y. Moritomo, A. Asamitsu, and Y. Tokura, Phys. Rev. B **56**, 12 190 (1997).
[3] Y. Yamada, O. Hino, S. Nohdo, R. Kanao, T. Inami, and S. Katano, Phys. Rev. Lett. **77**, 904 (1996).
[4] Y. Endoh, K. Hirota, S. Ishihara, S. Okamoto, Y. Murakami, A. Nishizawa, T. Fukuda, H. Kimura, H. Nojiri, K. Kaneko, and S. Maekawa, Phys. Rev. Lett. **82**, 4328 (1999).
[5] S. Uhlenbruck, R. Teipen, R. Klingeler, B. Büchner, O. Friedt, M. Hücker, H. Kierspel, T. Niemöller, L. Pinsard, A. Revcolevschi, and R. Gross, Phys. Rev. Lett. **82**, 185 (1999).
[6] B. Dabrowski, X. Xiong, Z. Bukowski, R. Dybzinski, P.W. Klamut, J.E. Siewenie, O. Chmaissem, J. Shaffer, C.W. Kimball, J.D. Jorgensen, and S. Short, Phys. Rev. B **60**, 7006 (1999).
[7] H. Kawano, R. Kajimoto, M. Kubota, and H. Yoshizawa, Phys. Rev. B **53**, R14 709 (1996).
[8] S.J.L. Billinge, R.G. DiFrancesco, G.H. Kwei, J.J. Neumeier, and J.D. Thompson, Phys. Rev. Lett. **77**, 715 (1996).
[9] P. Dai, J.A. Fernandez-Baca, N. Wakabayashi, E.W. Plummer, Y. Tomioka, and Y. Tokura, Phys. Rev. Lett. **85**, 2553 (2000).
[10] J.-S. Zhou, J.B. Goodenough, A. Asamitsu, and Y. Tokura, Phys. Rev. Lett. **79**, 3234 (1997); J.-S. Zhou and J.B. Goodenough, Phys. Rev. B **62**, 3834 (2000).
[11] H. Nojiri, K. Kaneko, M. Motokawa, K. Hirota, Y. Endoh, and K. Takahashi, Phys. Rev. B **60**, 4142 (1999).
[12] M. Paraskevopoulos, F. Mayr, J. Hemberger, A. Loidl, R. Heichele, D. Maurer, V. Müller, A.A. Mukhin, and A.M. Balbashov, J. Phys.: Condens. Matter **12**, 3993 (2000).
[13] J.-S. Zhou, G.-L. Liu, and J.B. Goodenough, Phys. Rev. B **63**, 172416 (2001).
[14] I. El-Kassab, A.M. Ahmed, P. Mandal, K. Bärner, A. Kattwinkel, and U. Sondermann, Physica B **305**, 233 (2001).
[15] A.A. Mukhin, V.Yu. Ivanov, V.D. Travkin, and S.P. Lebedev, A. Pimenov, A. Loidl, and A.M. Balbashov, JETP Lett. **68**, 356 (1998).
[16] R. Klingeler, J. Geck, R. Gross, L. Pinsard-Gaudart, A. Revcolevschi, S. Uhlenbruck, and B. Büchner, Phys. Rev. B **65**, 174404 (2002).
[17] B. Dabrowski, K. Rogacki, X. Xiong, P.W. Klamut, R. Dybzinski, J. Shaffer, and J.D. Jorgensen, Phys. Rev. B **58**, 2716 (1998).
[18] H.L. Ju, Y.S. Nam, J.E. Lee, and H.S. Shin, J. Magn. Magn. Mater. **219**, 1 (2000).
[19] T. Okuda, Y. Tomioka, A. Asamitsu, and Y. Tokura, Phys. Rev. B **61**, 8009 (2000); C.S. Hong, W.S. Kim, and N.H. Hur, *ibid.* **63**, 092504 (2001); J. Dho, I. Kim, S. Lee, K.H. Kim, H.J. Lee, J.H. Jung, and T.W. Noh, *ibid.* **59**, 492 (1999).
[20] P. Mandal, B. Bandyopadhyay, and B. Ghosh, Phys. Rev. B **64**, 180405 (2001).
[21] X.J. Chen, S. Soltan, H. Zhang, and H.-U. Habermeier, Phys. Rev. B **65**, 174402 (2002).
[22] G.Y. Snyder, M.R. Beasley, and T.H. Geballe, Appl. Phys. Lett. **69**, 4254 (1996).
[23] L. Wang, J. Yin, S. Huang, X. Huang, J. Xu, Z. Liu, and K. Chen, Phys. Rev. B **60**, 6976 (1999).
[24] M. Jaime, M.B. Salamon, M. Rubinstein, R.E. Treece, J.S. Horwiz, and D.B. Chrisey, Phys. Rev. B **54**, 11 914 (1996).
[25] M. Jaime, H.T. Hardner, M.B. Salamon, M. Rubinstein, P. Dorsey, and D. Emin, Phys. Rev. Lett. **78**, 951 (1997).
[26] D. Emin and T. Holstein, Ann. Phys. (N.Y.) **53**, 439 (1969).
[27] I.G. Austin and N.F. Mott, Adv. Phys. **18**, 41 (1969).
[28] G. Biotteau, M. Hennion, F. Moussa, J. Rodriguez-Carvajal, L. Pinsard, A. Revcolevschi, Y.M. Mukovskii, and D. Shulyatev, Phys. Rev. B **64**, 104421 (2001).
[29] L.M. Rodriguez-Martinez and J.P. Attfield, Phys. Rev. B **54**, R15 622 (1996).
[30] R.D. Shannon, Acta Crystallogr., Sect. A: Cryst. Phys., Diffr., Theor. Gen. Crystallogr. **32**, 751 (1976).
[31] J. Rodriguez-Carvajal, M. Hennion, F. Moussa, A. Moudden, L. Pinsard, and A. Revcolevschi, Phys. Rev. B **57**, R3189 (1998).
[32] T. Chatterjee, B. Ouladdiaf, P. Mandal, B. Bandyopadhyay, and B. Ghosh, Phys. Rev. B **66**, 054403 (2002).
[33] O. Chmaissem, B. Dabrowski, S. Kolesnik, J. Mais, D.E. Brown, R. Kruk, P. Prior, B. Pyles, and J.D. Jorgensen, Phys. Rev. B **64**, 134412 (2001).